Nanoparticle Assemblies Hot Paper

DOI: 10.1002/anie.201306009

A Directional Entropic Force Approach to Assemble Anisotropic Nanoparticles into Superlattices**

Kaylie L. Young, Michelle L. Personick, Michael Engel, Pablo F. Damasceno, Stacey N. Barnaby, Reiner Bleher, Tao Li, Sharon C. Glotzer, Byeongdu Lee,* and Chad A. Mirkin**

Learning how to assemble inorganic nanoparticles into ordered lattices may prove to be important for applications, such as, electronics, photonics, and catalysis.[1] Indeed, theoretical studies have shown that certain types of crystalline arrays of nanoparticles could potentially be used to generate photonic band-gap materials, negative index materials, and metamaterials at visible and infrared length scales.[2,3] The vast majority of work in this area has focused on the assembly of spherical particles. However, anisotropic nanoparticles, which display rich assembly behavior owing to their reduced symmetry, and have unique physical properties that can be engineered by controlling interparticle spacing and orientation, may provide access to even more interesting materials.[4–8] Moreover, they require design rules for predicting the way such nanoparticles can assemble and the types of structures that may be realized. The rapidly expanding library of available anisotropic nanoparticle building blocks provides exciting new opportunities to study colloidal assembly as a function of particle shape.[9–11]

Herein, we introduce a directional entropic force approach (DEFA) for controlling the assembly of anisotropic nanoparticles into crystalline lattices. The method relies on surfactant micelle-induced depletion interactions[12] to assemble anisotropic gold nanoparticles into reconfigurable, non-close-packed (open) superlattices in solution. The anisotropic nanoparticles align along their flat facets to maximize entropy, and therefore minimize the free energy of the system, leading to assemblies with long-range order.[13,14] Importantly, our experimental work complements recent theoretical work that proposes directional entropic forces between nanoparticle facets as a viable means for thermodynamically assembling nanoparticle superlattices.[14–17] The experimental work herein uses depletants to create strong attractive forces that can drive assembly of reversible superlattices with tunable spacing in solution. These directional entropic forces are analogous to the directional bonding between atoms in molecules.[14,15,18] The resulting crystalline superlattices are therefore shape-dependent. We show that the electrostatic and depletion interactions combine to determine the lattice spacing, and can be tuned independently with surfactant concentration and ionic strength to reconfigure the lattice constant.

The DEFA presented herein complements several assembly strategies that have been developed to create superlattices of anisotropic nanostructures including evaporation-induced[19,20] and sedimentation-based methods,[8] as well as ones based upon the manipulation of electrostatic,[21,22] entropic,[13,23–28] block copolymer,[29,30] and biological recognition interactions.[31] However, unlike the majority of these methods, our approach yields reversible crystals with tunable lattice constants in situ.

Depletion interactions are purely entropic in nature and arise when non-adsorbing macromolecules, such as polymers or surfactants, are added to a stable colloidal solution.[32,33] Each particle in solution is surrounded by an exclusion zone with a thickness corresponding to the radius of the macromolecule. When two particles approach each other at a distance smaller than the diameter of the macromolecules

[*] Dr. K. L. Young, Dr. M. L. Personick, S. N. Barnaby, Prof. C. A. Mirkin
Department of Chemistry and International Institute for Nanotechnology, Northwestern University
2145 Sheridan Road, Evanston, IL 60208 (USA)
E-mail: chadnano@northwestern.edu
Dr. R. Bleher, Prof. C. A. Mirkin
Department of Materials Science and Engineering
Northwestern University
2200 Campus Drive, Evanston, IL 60208 (USA)
Dr. T. Li, Dr. B. Lee
X-ray Science Division, Argonne National Laboratory
9700 South Cass Avenue, Argonne, IL 60439 (USA)
E-mail: blee@anl.gov
Dr. M. Engel, P. F. Damasceno, Prof. S. C. Glotzer
Department of Chemical Engineering, Department of Materials Science & Engineering, Applied Physics Program, University of Michigan, North Campus Research Complex
2800 Plymouth Road, Ann Arbor, MI 48109 (USA)
E-mail: sglotzer@umich.edu

[**] C.A.M. and S.C.G. acknowledge the Department of Energy Office (DOE Award DE-SC0000989) for support through the Northwestern University Non-Equilibrium Energy Research Center. K.L.Y., M.L.P., and S.N.B. acknowledge support from the NSF through the Graduate Research Fellowship Program. K.L.Y. also acknowledges the NDSEG Fellowship. P.F.D, M.E., and S.C.G. acknowledge support from the U.S. Army Research Office under Grant Award No. W911NF-10-1-0518 and the U.S. Department of Defense ASD (R&E) under Award No. N00244-09-1-0062. Use of the Advanced Photon Source was supported by the Office of Basic Energy Sciences, US DOE under Contract DE-AC02-06CH11357. Electron microscopy was carried out in the Electron Probe Instrumentation Center facility of the Northwestern University Atomic and Nanoscale Characterization Experimental Center.

Supporting information for this article is available on the WWW under http://dx.doi.org/10.1002/anie.201306009.

(depletants), the macromolecules are excluded from the volume between the particles. A region of pure (i.e. depleted) solvent is generated between the particles, resulting in an osmotic pressure imbalance that pushes the particles together. The strength of the interaction scales according to the volume gained by bringing two particles together (ΔV), and therefore depletion forces are particularly attractive for assembling anisotropic building blocks due to their potential for a more efficient overlap of their exclusion layers compared to spherical building blocks.[34] Additionally, depletion interactions are maximized for smooth surfaces since less free volume is gained when two rough surfaces approach one another.[13,35] Herein we show that directional entropic depletion interactions can be used to induce the face-to-face assembly of anisotropic nanoparticles into superlattices, thereby providing a method to control the particle orientation and spatial arrangement of non-spherical building blocks in periodic structures.

Recently we demonstrated that triangular gold nanoprisms, which are an extreme example of an anisotropic nanoparticle with two large flat (111) faces, spontaneously assemble face-to-face into one-dimensional (1D) lamellar superlattices in solution as a result of surfactant micelle-induced depletion interactions.[12] Herein, we extend the concept of directional entropic depletion forces and study the assembly behavior of 3D polyhedra with flat facets: three isometric Au nanoparticle shapes including rhombic dodecahedra (RD), truncated cubes, and octahedra, as well as non-isometric rod-like tetrahexahedra (THH), exhibiting face-centered cubic (FCC), simple cubic (SC), body-centered cubic (BCC), and hexagonal assembly behavior in solution, respectively (Figure 1). The anisotropic nanoparticles were synthesized using reported procedures (Supporting Information).[10,36,37] Each of the syntheses requires the use of a cationic surfactant well above its critical micelle concentration (cmc): cetyltrimethylammonium chloride (CTAC, cmc = 0.8 mM)[38] for RD and cetyltrimethylammonium bromide (CTAB, cmc = 1.0 mM)[39] for octahedra, truncated cubes, and THH. A minute amount of the surfactant forms a stabilizing bilayer on the surface of the particles,[40] but the majority of the surfactant forms micelles (ca. 6 nm in diameter)[12] which serve as the depletants that cause the assembly of the nanocrystals in solution. The charge of the surfactant bilayer and micelles results in long-range electrostatic repulsions that greatly increase both the magnitude and the range of the depletion effect.[41] The interparticle spacing of particles within the superlattices is thus determined by a balance between attractive depletion interactions and repulsive electrostatic interactions.[12]

The assembled superlattices were characterized by in situ synchrotron small angle X-ray scattering (SAXS) and compared to the scattering patterns of the analogous atomic lattices. A wealth of information about the superlattices can be obtained from the SAXS patterns including the crystallographic symmetry, lattice parameters, and particle orientation.[42] Additionally, cryo-electron microscopy, Monte Carlo assembly simulations, and modeling of powder diffraction patterns were used to support the conclusions made based on the SAXS data (Supporting Information).

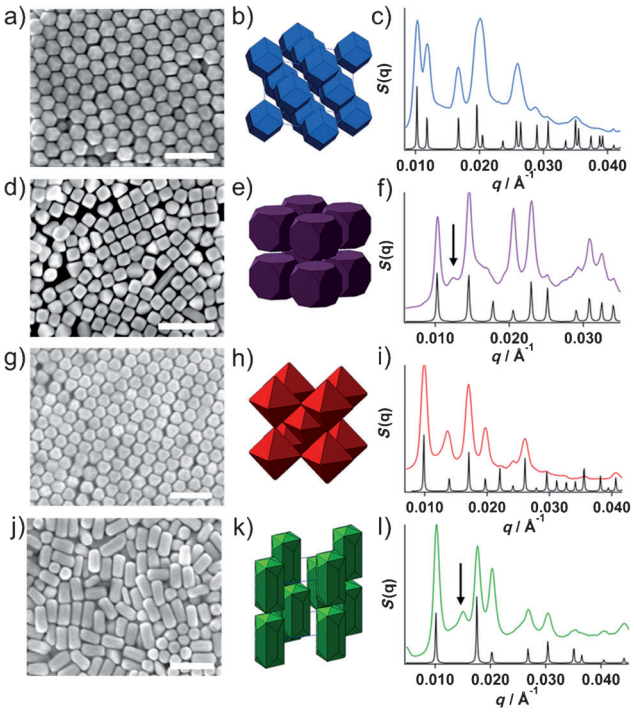

Figure 1. Characterization of anisotropic nanoparticles and the superlattices they form in solution. Nanoparticle geometries are rhombic dodecahedra (a–c), truncated cubes (d–f), octahedra (g–i), and tetrahexahedra (j–l). First column: SEM images of (unassembled) particles in the dried state. Second column: Representation of the unit cells formed when the particles assemble. The nanoparticles may have a distribution of orientations within some crystals. Third column: Experimental (colored) and modeled (black) SAXS patterns for the assemblies. Note that the modeled SAXS patterns are the calculated lattice factors which take only the position of the scatterers into account, not their shape (Supporting Information and Figure S8). The arrows denote peaks that do not match with the modeled SAXS patterns and are discussed in the text. Scale bars: 200 nm.

Interestingly, the RD particles assemble into non-close-packed superlattices that are stable in solution directly from synthesis and without further modification. Since RD particles are bound by twelve identical (110) facets, the maximum overlap volume is predicted to be obtained when the particles arrange into an FCC lattice with their (110) facets aligned. At a CTAC surfactant concentration of 0.08 M (100 times the cmc, hereafter referred to as 100 × cmc), the RD (edge length 36.3 ± 2.7 nm) indeed arrange into 3D superlattices with FCC symmetry and orientational order, where each (110) plane of the RD becomes a (110) plane in the superlattice, as confirmed by SAXS and cryo-electron microscopy (Figure 1 b,c and Figure S1). The large number of sharp diffraction peaks is indicative of highly ordered crystals with domain sizes on the micron scale (Table S2). The degree of order that is observed for the RD superlattices is remarkable given the lack of covalent bonds between the individual components, but is in agreement with theoretical predictions.[14] Importantly, the faces of the RD are not in contact and instead the RD have a center-to-center distance (d-spacing) of 74.6 nm, corresponding to a gap of 15.3 nm between the (110) faces of neighboring RD (Table 1). This gap size is almost identical to that observed for triangular nanoprisms that arrange into

Table 1: Dimensions of anisotropic nanoparticles and their interparticle distances within superlattices formed using the DEFA.

Nanoparticle[a]	NP edge length [nm]	NP center-to-face distance [nm]	Nearest-neighbor distance[b] [nm]	Gap size between faces [nm]
RD	36.3	29.6	74.6	15.3
Truncated cubes	46.6	23.3	61.2	14.6
Octahedra	70.0	28.6	78.0	20.8
THH	41.2	27.0	71.5	17.4

[a] RD = rhombic dodecahedra, THH = tetrahexahedra. [b] Values were calculated from the SAXS data.

lamellar stacks with alignment of their flat (111) facets at a comparable surfactant concentration (16.8 nm gap, 100× cmc of CTAB), indicating that the gap can be predicted by the pair-potential between two flat faces.[12] These data suggest that while the symmetry of the superlattices is determined by shape, the gap size is determined by a competition between electrostatics and depletion by the charged surfactants, which serve as both the ligands and the micelles. The other polyhedra that we investigated follow the same principles, although the presence of truncated and sharp corners in truncated cubes and octahedra, respectively, plays a role in the gap size (see below).

The directional entropic forces between nanoparticle building blocks are tunable and reversible by manipulating the balance of interparticle interactions. The strength of the depletion interaction can be increased by an increase in the number density of the surfactant micelles, which serves to increase the osmotic pressure imbalance that causes the nanoparticles to assemble. The RD were used as a model system to demonstrate the tunability of the lattice spacing of the depletion-induced assemblies. CTAC was added incrementally from 0.024 M (30× cmc) to a final concentration of 0.400 M (500× cmc). As shown in Figure 2a, the diffraction peaks shifted to higher values of the scattering vector q with each addition of CTAC, indicative of smaller d-spacings between the RD. The d-spacing between RD was tunable from 75.3 to 72.3 nm (gap size 16 to 13 nm; Figure 2b). Conversely, dilution of the CTAC concentration led to an increase in the d-spacing and eventual dissociation of the FCC superlattices at a critical surfactant concentration, below which the depletion interactions are no longer strong enough to cause assembly. For the RD, the critical CTAC concentration was determined to be 0.032 M, 40× cmc of CTAC. Below 0.032 M CTAC, the SAXS patterns contain only form factor scattering from the RD (Figure 2a). The d-spacing between the RD was also tunable by changing the ionic strength of the solution through the addition of NaCl, thereby screening the electrostatic interactions that exist between the positively charged RD and leading to a decrease in the interparticle spacing (Figure 2b). Interestingly, the RD exhibit a dampening and blue-shift of their surface plasmon resonance when assembled compared to when they are dispersed in solution, which is opposite of the red-shift observed when spherical particles assemble (Figure S2).[43] The reason for the blue shift is still under investigation.

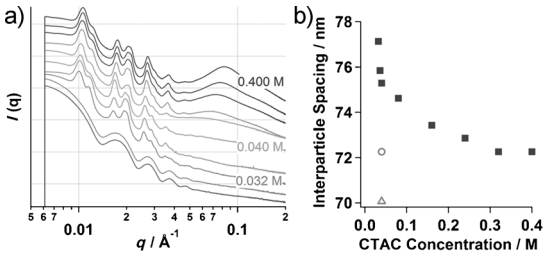

Figure 2. Tunability of anisotropic nanoparticle superlattices assembled using the DEFA. a) SAXS profiles of RD as the CTAC surfactant concentration was increased from 0.024 M (30× cmc; bottom) to 0.400 M (500× cmc; top). The diffraction peaks shift to higher q values at higher surfactant concentrations, indicating a decrease in the interparticle distance. b) Interparticle spacing (center-to-center) of neighboring RD as a function of CTAC concentration (filled squares). The open symbols indicate the interparticle spacing when NaCl is added to the solution to create a final concentration of 0.15 M (open circle) and 0.30 M (open triangle), respectively, at 0.04 M CTAC.

Truncated cubes and octahedra are interesting building blocks for nanoparticle assemblies because their calculated densest lattice packings do not maximize face-to-face contact.[14,15,44] The truncated cubes are bound by six (100) facets with an edge length of 46.6 ± 2.7 nm and their eight corners are truncated approximately 30%, revealing small (111) facets.[10] The octahedra are bound by eight (111) facets with an edge length of 70.0 ± 3.8 nm (the tips have less than 5% truncation and are therefore not referred to as truncated).[10] For depletion-based assembly, entropy maximization favors mutual alignment of particles along their flat facets and therefore we hypothesized that both of these nanoparticles would form superlattices that maximized alignment of their facets: SC for truncated cubes and BCC for octahedra. At the same CTAB concentration (0.1 M, 100× cmc), the truncated cubes assembled in register into a SC lattice (Figure 1e,f), allowing for maximum alignment of the (100) facets. The extra peak between the first and second order peaks in the SAXS pattern (denoted with an arrow) is believed to originate from minor domains with a slightly distorted SC structure (Figure S3).[24] Based on the SAXS data, the truncated cubes had an interparticle spacing (center-to-center) of 61.2 nm, corresponding to a gap size of 14.6 nm (Table 1). The slightly decreased gap size compared to that of the RD and nanoprisms is believed to be a result of the slightly decreased electrostatic repulsion that occurs owing to the pore that forms when eight truncated cubes come together (Figure S4a).[24] Owing to the extra volume, the distance between the (111) facets is longer than that between the (100) facets, and as a result, the particles are "pulled together" along the (111) facets, leading to a shorter gap size overall.

The octahedra show the opposite effect: their sharp edges cause a larger gap size. At 0.1 M CTAB (100× cmc), the octahedra assembled into a BCC lattice (Figure 1h,i). The octahedra may have orientational defects within the BCC lattice.[14] The depletion-induced exclusion zone around each octahedron overlaps with the exclusion zone of neighboring particles, so as to maximize face-to-face interactions, which can only be accomplished by forming a BCC arrangement.[14,15,31] The distance between the centers of the octahe-

dra was determined to be 78.0 nm, with a gap size of 20.8 nm (Table 1). When octahedra assemble into a BCC arrangement, the exclusion zones at their sharp tips overlap to a greater degree than anywhere else along the (111) facets (Figure S4b). As a result, the repulsion between octahedra is greater than that between particles that do not have overlapping corners, such as RD and nanoprisms, and a larger gap between the (111) facets results. Importantly, 60 nm spherical nanoparticles did not assemble into superlattices under the conditions used to assemble the anisotropic particles, demonstrating the importance of flat facets in the DEFA (Figure S5).

Simulations confirm that the superlattices formed by RD, truncated cubes, and octahedra are entropically stabilized (Figure S9 a–c). Electrostatic repulsions set the lattice spacing for these shapes, but not the lattice symmetry. Competition between directional entropic forces and other forces, such as electrostatic repulsion, can also determine the lattice symmetry, as is seen in the structures formed by THH particles. THH are nanoparticles with twenty four high-index facets of the (730) family, eight of which are trapezoid-shaped when the particles have an aspect ratio greater than one.[37] The THH we synthesized had an aspect ratio of approximately 2, with a length of 107.0 ± 11.5 nm and a width of 54.1 ± 4.5 nm (between trapezoid planes, 58.8 nm between opposite tips). Due to their elongated shape, we hypothesized that THH particles would preferentially assemble via lateral association, with their long axes aligned parallel in order to maximize the excluded volume ΔV, similar to what has been observed for cylinders and nanorods.[25,31] Indeed, SAXS analysis for the THH with $100 \times$ cmc CTAB (as-synthesized) revealed a diffraction pattern that resembles a 2D hexagonal lattice (Figure 1 k,l). Based on the SAXS data, the hexagonal unit cell of the THH particles is calculated to have a lattice parameter of 71.5 nm. Although the hexagonal arrangement may be the densest packing structure for rod-like particles, the octagonal cross section of the THH greatly reduces their packing efficiency compared to rods with a hexagonal cross section. While the extra volume between the THH results in the particles being "pulled together," similar to the truncated cubes, the sharp edges between neighboring THH are repulsive, similar to the octahedra. The gap between the trapezoidal faces of neighboring THH was calculated to be 17.4 nm (Table 1), and the distance between their edges was 12.7 nm. Considering the large gap sizes observed for the octahedra, the edge-to-edge repulsion of the THH is believed to be compensated by the attraction owing to the extra volume between THH.

Note that the SAXS pattern in Figure 1l contains an extra peak between the first and second order peaks (denoted with an arrow), and the position of this peak shifts slightly at different locations within the sample (Figure 3). The extra peak indicates a correlation between THH along their long axes. While the broad diffraction peaks limit the determination of the exact symmetry along the *c*-direction, the existence of a set of peaks indexed to a 2D hexagonal lattice and the absence of any lamellar peaks suggest that the THH do not form a lamellar structure. Examination of the 2D SAXS data and cryo-electron microscopy images (Figure S6)

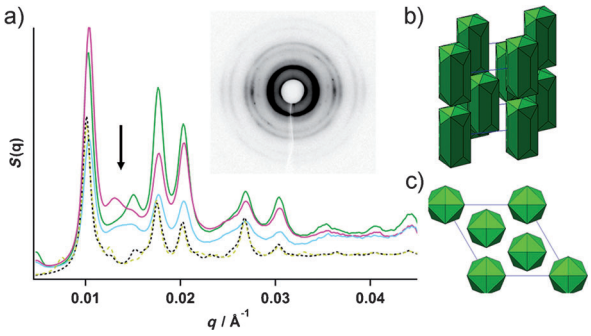

Figure 3. Characterization of hexagonal lattices of THH with ABC-type packing. a) SAXS profiles of THH superlattices collected at three different locations within the capillary containing the sample (solid green, pink, and light blue lines). The position and intensity of the out-of-plane diffraction peak (denoted with an arrow) change with location. The dotted lines are simulated SAXS patterns for different lattice parameters for the *c*-axis (black = 125 nm and gold = 135 nm). The in-plane diffraction peaks resulting from the hexagonally arranged THH do not shift. Inset: 2D SAXS pattern for the pink curve. Schematic representation of a side view (b) and a top-down view (c) of the THH superlattices.

suggest that the THH pack into 3D hierarchical structures that are unique compared to nanorods. This effect may be due to the extruded edges of the THH, which hinder them from freely sliding along one another in the vertical direction. The experimental SAXS data suggest that the hexagonally arranged THH assemble tip-to-tip with "ABC-type" packing, where the length of the *c*-axis and the stacking order may vary at different points within a sample, leading to the diffuse peaks in the 1D SAXS patterns. Simulated SAXS patterns for the arrays of THH with ABC-type packing along their long axes are in good agreement with the experimental data (Figure 3). Interestingly, simulations based on entropy alone do not predict that the THH will form such assemblies, and instead suggest that the THH form hexagonal arrangements that organize into a lamellar structure with ABC-type stacking (Supporting Information). This discrepancy between experiment and theory and the role of additional interactions is currently being explored. An equal ratio mixture of THH and RD resulted in phase separation and formation of 2D hexagonal assemblies of THH and 3D assemblies of RD with an FCC lattice in solution (Figure S7), confirming the trend towards maximization of face-to-face alignment since in this instance the magnitude of ΔV is larger when particles of the same shape come together.[34]

In conclusion, we have shown that surfactant-micelle induced depletion interactions can be used to assemble anisotropic nanoparticles into superlattices in solution with positional and orientational order. Through entropy maximization, the shape anisotropy of the building blocks can be exploited to program and regulate their assembly: the shape of the particle determines the crystallographic symmetry of the resulting superlattice, but the gap size is determined by the competition of depletion and electrostatic interactions. The use of the DEFA to assemble anisotropic nanoparticles bypasses the need for covalent bonds between building blocks and leads to superlattices that are reconfigurable by tuning

the strength of the interparticle forces, thereby allowing for a systematic study of structure–property relationships of nanoparticle superlattices. Our results confirm that faceted nanoparticles can be used as "smart" building blocks that are capable of binding specificity by directional and reversible interactions, making them attractive building blocks for designer materials. Furthermore, owing to the structural lability of nanoparticles assembled by directional entropic forces, the use of the superlattices to create non-equilibrium structures with interesting properties that are not possible at thermal equilibrium can be envisaged.[45]

Received: July 10, 2013
Published online: November 7, 2013

Keywords: depletion forces · entropy · nanomaterials · nanoparticles · surfactants

[1] Z. Nie, A. Petukhova, E. Kumacheva, *Nat. Nanotechnol.* **2010**, *5*, 15 – 25.
[2] M. J. Solomon, *Curr. Opin. Colloid Interface Sci.* **2011**, *16*, 158 – 167.
[3] K. J. Stebe, E. Lewandowski, M. Ghosh, *Science* **2009**, *325*, 159 – 160.
[4] S. C. Glotzer, M. J. Solomon, *Nat. Mater.* **2007**, *6*, 557 – 562.
[5] Z. Quan, J. Fang, *Nano Today* **2010**, *5*, 390 – 411.
[6] A. Tao, P. Sinsermsuksakul, P. Yang, *Nat. Nanotechnol.* **2007**, *2*, 435 – 440.
[7] X. Ye, J. Chen, M. Engel, J. A. Millan, W. Li, L. Qi, G. Xing, J. E. Collins, C. R. Kagan, J. Li, S. C. Glotzer, C. B. Murray, *Nat. Chem.* **2013**, *5*, 466 – 473.
[8] J. Henzie, M. Grünwald, A. Widmer-Cooper, P. L. Geissler, P. Yang, *Nat. Mater.* **2012**, *11*, 131 – 137.
[9] S. Sacanna, D. J. Pine, *Curr. Opin. Colloid Interface Sci.* **2011**, *16*, 96 – 105.
[10] M. R. Langille, M. L. Personick, J. Zhang, C. A. Mirkin, *J. Am. Chem. Soc.* **2012**, *134*, 14542 – 14554.
[11] Y. Xia, Y. Xiong, B. Lim, S. E. Skrabalak, *Angew. Chem.* **2009**, *121*, 62 – 108; *Angew. Chem. Int. Ed.* **2009**, *48*, 60 – 103.
[12] K. L. Young, M. R. Jones, J. Zhang, R. J. Macfarlane, R. Esquivel-Sirvent, R. J. Nap, J. Wu, G. C. Schatz, B. Lee, C. A. Mirkin, *Proc. Natl. Acad. Sci. USA* **2012**, *109*, 2240 – 2245.
[13] E. Barry, Z. Dogic, *Proc. Natl. Acad. Sci. USA* **2010**, *107*, 10348 – 10353.
[14] P. F. Damasceno, M. Engel, S. C. Glotzer, *Science* **2012**, *337*, 453 – 457.
[15] P. F. Damasceno, M. Engel, S. C. Glotzer, *ACS Nano* **2011**, *6*, 609 – 614.
[16] G. van Anders, N. K. Ahmed, R. Smith, M. Engel, S. C. Glotzer, *arXiv:1304.7545 [cond-mat.soft]* **2013**.
[17] G. van Anders, N. K. Ahmed, D. Klotsa, M. Engel, S. C. Glotzer, *arXiv:1309.1187 [cond-mat.soft]* **2013**.
[18] B. J. Holliday, C. A. Mirkin, *Angew. Chem.* **2001**, *113*, 2076 – 2097; *Angew. Chem. Int. Ed.* **2001**, *40*, 2022 – 2043.
[19] T. Ming, X. Kou, H. Chen, T. Wang, H.-L. Tam, K.-W. Cheah, J.-Y. Chen, J. Wang, *Angew. Chem.* **2008**, *120*, 9831 – 9836; *Angew. Chem. Int. Ed.* **2008**, *47*, 9685 – 9690.
[20] T. Huang, Q. Zhao, J. Xiao, L. Qi, *ACS Nano* **2010**, *4*, 4707 – 4716.
[21] A. M. Kalsin, M. Fialkowski, M. Paszewski, S. K. Smoukov, K. J. M. Bishop, B. A. Grzybowski, *Science* **2006**, *312*, 420 – 424.
[22] E. V. Shevchenko, D. V. Talapin, N. A. Kotov, S. O'Brien, C. B. Murray, *Nature* **2006**, *439*, 55 – 59.
[23] S. Sacanna, W. T. M. Irvine, P. M. Chaikin, D. J. Pine, *Nature* **2010**, *464*, 575 – 578.
[24] L. Rossi, S. Sacanna, W. T. M. Irvine, P. M. Chaikin, D. J. Pine, A. P. Philipse, *Soft Matter* **2011**, *7*, 4139 – 4142.
[25] D. Baranov, A. Fiore, M. van Huis, C. Giannini, A. Falqui, U. Lafont, H. Zandbergen, M. Zanella, R. Cingolani, L. Manna, *Nano Lett.* **2010**, *10*, 743 – 749.
[26] M. Zanella, G. Bertoni, I. R. Franchini, R. Brescia, D. Baranov, L. Manna, *Chem. Commun.* **2011**, *47*, 203 – 205.
[27] T. Li, R. E. Winans, B. Lee, *Langmuir* **2011**, *27*, 10929 – 10937.
[28] T. Li, X. Zan, R. E. Winans, Q. Wang, B. Lee, *Angew. Chem.* **2013**, *125*, 6770 – 6774; *Angew. Chem. Int. Ed.* **2013**, *52*, 6638 – 6642.
[29] Z. Nie, D. Fava, E. Kumacheva, S. Zou, G. C. Walker, M. Rubinstein, *Nat. Mater.* **2007**, *6*, 609 – 614.
[30] D. Fava, Z. Nie, M. A. Winnik, E. Kumacheva, *Adv. Mater.* **2008**, *20*, 4318 – 4322.
[31] M. R. Jones, R. J. Macfarlane, B. Lee, J. Zhang, K. L. Young, A. J. Senesi, C. A. Mirkin, *Nat. Mater.* **2010**, *9*, 913 – 917.
[32] S. Asakura, F. Oosawa, *J. Chem. Phys.* **1954**, *22*, 1255 – 1256.
[33] K. J. M. Bishop, C. E. Wilmer, S. Soh, B. A. Grzybowski, *Small* **2009**, *5*, 1600 – 1630.
[34] T. G. Mason, *Phys. Rev. E* **2002**, *66*, 060402.
[35] K. Zhao, T. G. Mason, *Phys. Rev. Lett.* **2007**, *99*, 268301.
[36] M. L. Personick, M. R. Langille, J. Zhang, N. Harris, G. C. Schatz, C. A. Mirkin, *J. Am. Chem. Soc.* **2011**, *133*, 6170 – 6173.
[37] T. Ming, W. Feng, Q. Tang, F. Wang, L. Sun, J. Wang, C. Yan, *J. Am. Chem. Soc.* **2009**, *131*, 16350 – 16351.
[38] E. Roelants, F. C. De Schryver, *Langmuir* **1987**, *3*, 209 – 214.
[39] R. M. Pashley, P. M. McGuiggan, R. G. Horn, B. W. Ninham, *J. Colloid Interface Sci.* **1988**, *126*, 569 – 578.
[40] K. Park, H. Koerner, R. A. Vaia, *Nano Lett.* **2010**, *10*, 1433 – 1439.
[41] J. Y. Walz, A. Sharma, *J. Colloid Interface Sci.* **1994**, *168*, 485 – 496.
[42] R.-J. Roe, *Methods of X-ray and Neutron Scattering in Polymer Science*, Oxford University Press, New York, **2000**.
[43] C. A. Mirkin, R. L. Letsinger, R. C. Mucic, J. J. Storhoff, *Nature* **1996**, *382*, 607 – 609.
[44] S. Torquato, Y. Jiao, *Nature* **2009**, *460*, 876 – 879.
[45] A. S. Mikhailov, G. Ertl, *Science* **1996**, *272*, 1596 – 1597.

